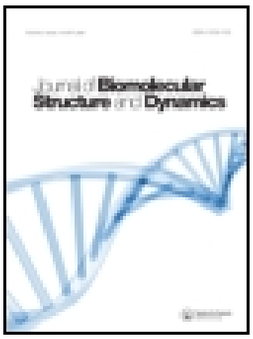

Taylor & Francis
Taylor & Francis Group

Journal of Biomolecular Structure and Dynamics

ISSN: (Print) (Online) Journal homepage: https://www.tandfonline.com/loi/tbsd20

Interaction between escitalopram and ibuprofen or paracetamol: DFT and molecular docking on the drug–drug interactions

Musa Daboe, Cemal Parlak, Amani Direm, Özgür Alver & Ponnadurai Ramasami

To cite this article: Musa Daboe, Cemal Parlak, Amani Direm, Özgür Alver & Ponnadurai Ramasami (2023): Interaction between escitalopram and ibuprofen or paracetamol: DFT and molecular docking on the drug–drug interactions, Journal of Biomolecular Structure and Dynamics, DOI: 10.1080/07391102.2023.2195004

To link to this article: https://doi.org/10.1080/07391102.2023.2195004

JOURNAL OF BIOMOLECULAR STRUCTURE AND DYNAMICS
https://doi.org/10.1080/07391102.2023.2195004

Interaction between escitalopram and ibuprofen or paracetamol: DFT and molecular docking on the drug–drug interactions

Musa Daboe[a], Cemal Parlak[a], Amani Direm[b,c], Özgür Alver[d] and Ponnadurai Ramasami[e,f]

[a]Department of Physics, Science Faculty, Ege University, Izmir, Turkey; [b]Department of Matter Sciences, Faculty of Sciences and Technology, Abbes Laghrour University, Khenchela, Algeria; [c]Laboratory of Structures, Properties and Interatomic Interactions LASPI2A, Faculty of Sciences and Technology, Abbes Laghrour University, Khenchela, Algeria; [d]Department of Physics, Science Faculty, Eskişehir Technical University, Eskişehir, Turkey; [e]Computational Chemistry Group, Department of Chemistry, Faculty of Science, University of Mauritius, Réduit, Mauritius; [f]Department of Chemistry College of Science, Engineering and Technology, University of South Africa, Pretoria, South Africa

Communicated by Ramaswamy H. Sarma

ABSTRACT

A large number of drugs are introduced each year to treat different diseases. Most of the time, patients suffer from more than one health problem which makes it necessary to take multiple drugs. When drugs are combined, the problem of drug–drug interaction becomes relevant. In this work, we studied the drug–drug interaction between escitalopram and ibuprofen or paracetamol using density functional theory and quantum theory of atoms in molecules. The results suggest that following the interactions, the activity of drugs changes according to site of interaction. Most reactive and most stable interactions would be preferable for the purpose of use. The *in silico* drug-likeness studies show that escitalopram and paracetamol couple is more bioavailable than escitalopram and ibuprofen couple. Moreover, in order to gain additional insights into the mentioned drugs' interactions, the drugs were docked separately and jointly against the potential targets for antidepressants and NSAIDs, namely **6HIS** and **2PXX**. The molecular docking results showed a potential improvement of the effectiveness of the drugs after combining by forming hydrogen bonds, hydrophobic contacts and $\pi \ldots \pi$ stacking.

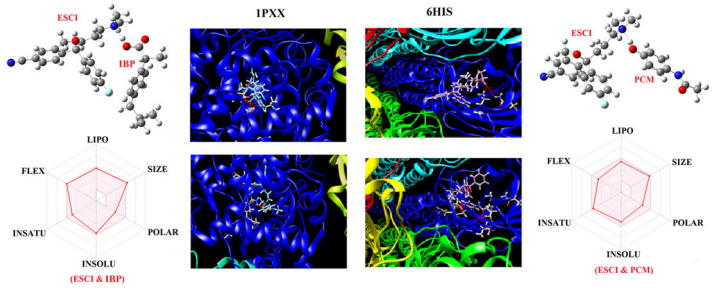

ARTICLE HISTORY
Received 13 September 2022
Accepted 17 March 2023

KEYWORDS
DFT; QTAIM; drug–drug interaction; molecular docking; $5HT_3$; COX-2

1. Introduction

The drug–drug interaction is known as the effect of one drug upon another. If more than one drug is taken by a patient at once, there appears a possibility of drug–drug interaction (Flynn, 2007). This interaction can be pharmacodynamic or pharmacokinetic and may produce desired or undesired results (Flynn, 2007). Pharmacodynamic drug interactions are known as the competition between two drugs for the same target molecule whereas pharmacokinetic drug interactions are mostly known as the change in the rate of elimination of one of the drugs in competition (Flynn, 2007). Furthermore, in certain circumstances such as postoperative pain, dysmenorrhea and musculoskeletal pain, the combination of drugs such as ibuprofen (IBP) and paracetamol (PCM) has been suggested as an effective method for the treatment (Derry et al., 2013; Doherty et al., 2011; Eccles et al., 2010). Drug interactions might refer to chemical or physical interactions. Since a large number of drugs come into the market each year, it appears as an important issue to know their interactions with other drugs.

2-(4-Isobutylphenyl) propionic acid also known as IBP is one of most prescribed drugs which is accepted for its well-known non-steroidal, anti-inflammatory, analgesic and antipyretic effects (Lazarević et al., 2014). It is also considered as an alternative to aspirin within the medicinal society. PCM,

CONTACT Ponnadurai Ramasami p.ramasami@uom.ac.mu Computational Chemistry Group, Department of Chemistry, Faculty of Science, University of Mauritius, Réduit, Mauritius

Supplemental data for this article can be accessed online at https://doi.org/10.1080/07391102.2023.2195004.

also known as acetaminophen, is also used for its analgesic, antipyretic and anti-inflammatory activities (Anderson, 2008; Langhendries et al., 2016). Like aspirin and IBP, it is among the widely used drugs. Since it has been introduced in 2002, escitalopram (ESCI) is known as a selective serotonin reuptake inhibitor and it has been prescribed for the treatment of depression, general anxiety and panic disorder (Jonathan et al., 2004; Owens et al., 2001). It is particularly effective and usually well tolerated even for the treatment of serious generalized anxiety problems (Dhillon et al., 2006).

Quantum chemical calculations are commonly used with sufficient accuracy for the investigation of molecular structure, electronic properties, understanding of chemical process and reactivity of different types of molecular compounds (Kraka & Cremer, 2000; Parlak et al., 2021; Reshmy et al., 2012). Among the computational applications, density functional theory (DFT) offers a compromise between accuracy and computational time (Cao et al., 2020; Kraka & Cremer, 2000). DFT uses electron density, ρ and the ground state energy to determine electronic properties of molecular systems (Hohenberg & Kohn, 1964). DFT has become an important part of drug design and drug delivery applications since it provides a very cost-effective and fast method for the pre-evaluation of potential drugs (Mirhaji et al., 2018; Najafi et al., 2019; Yoosefian et al., 2019). The difficulty of experimental studies for biological systems is very well known and thus DFT method is useful to find a relationship between structure and activity for a wide range of molecular systems (Mehdipour et al., 2009; Paulino et al., 2008). In general, the structure and activity relationship are obtained based on some important electronic parameters such as energies of the highest occupied and the lowest unoccupied molecular orbitals (E_{HOMO}—E_{LUMO}), chemical hardness (η) and electrophilicity index (ω) (Behzadi et al., 2015; Kawakami et al., 2013).

Quantum theory of atoms in molecules (QTAIM) proposed by Bader is widely applied to understand the covalent and non-covalent atom–atom interactions in various types of molecular systems from small molecular compounds to proteins and DNA (Bader, 1990; Grabowski, 2011; Hirano et al., 2016; Parthasarathi et al., 2004; 2005). It is also reported that electron densities obtained theoretically give insights into the nature of chemical bonding (Parthasarathi et al., 2005). In the assessment of the nature of bonding with the QTAIM methodology, there are several important parameters which are analyzed together to identify the bond characteristics. These are the electron density ρ, Laplacian of electron density $\nabla^2\rho$ and electronic energy density H (Bader, 1990). Together with ρ, $\nabla^2\rho$ and H, the ratio between the kinetic and the potential electron energy density $G(r)/|V(r)|$ is also important to understanding the nature of bonding. According to Rozas et al., the sign of the $\nabla^2\rho$ and H could be informative for the determination of the hydrogen bonding (HB) interactions (Rozas et al., 2000). Basically, if $\nabla^2\rho < 0$ and $H < 0$, the interaction is covalent or strong and if $\nabla^2\rho > 0$ and $H < 0$, the interaction is partially covalent or medium and if $\nabla^2\rho > 0$ and $H > 0$, the interaction is non-covalent or weak in nature (Rozas et al., 2000).

Vibrational spectroscopic investigations of different types of molecular systems based on computational methods have the potential to enlighten the intra- or intermolecular interactions including hydrogen bond (HB) interactions (Barone, 2011; Fornaro et al., 2015; Jensen & Bunker, 2000). HB interactions can be followed by observing the changes of frequency shifts and intensity of the bands involved in the hydrogen bonding (Fornaro et al., 2015). Therefore, vibrational spectroscopic analyses in the theoretical ground propose a very powerful method for the identification of HB interactions.

The 5-hydroxytryptamine type-3 receptor ($5HT_3$) belongs to the family of pentameric ligand-gated ion channels (pLGICs) which comprises, in mammals, activated serotonin, acetylcholine, glycine and γ-aminobutyric acid (Nemecz et al., 2016). In fact, the $5HT_3$ receptor has been linked to the improvement of health problems, such as depression (Fakhfouri et al., 2019) and body weight control (Oh et al., 2015; Weber et al., 2009). Furthermore, alosetron is clinically used to treat irritable bowel syndrome (Chey et al., 2015) and vortioxetine is one of the non-selective antidepressants which targets the serotonin transporter and receptors (Bang-Andersen et al., 2011). Cyclooxygenase COX known as prostaglandin endoperoxide synthase is the rate-limiting enzyme in the production of prostaglandin from arachidonic acid (Smith et al., 1996) and is mainly present as two isoforms COX-1 and COX-2. Actually, the role of COX in inflammation (Gandhi et al., 2017; Simon, 1999) and Alzheimer's disease (Hoozemans et al., 2003; McGeer, 2000) has well been elucidated. Recently, researchers have shown that COX-2 was overexpressed in several cancers, namely in the case of colon (Eberhart et al., 1994; Kargman et al., 1995), stomach (Ristimaki et al., 1997), breast (Parrett et al., 1997), lung (Hida et al., 1998), esophagus (Zimmermann et al., 1999), pancreas (Tucker et al., 1999), urinary bladder (Shirahama & Sakakura, 2001), prostate (Yoshimura et al., 2000), head and neck (Chan et al., 1999; Sakurai et al., 2001) cancers. In fact, several studies have shown a 40–50% decrease in relative risk for colorectal cancer in persons who regularly take aspirin and other non-steroidal anti-inflammatory drugs (NSAIDs) (Giovannucci et al., 1994; Thun et al., 1991). Additionally, clinical studies on humans have shown that celecoxib and rofecoxib are able to eliminate the pain without causing any significant gastroduodenal toxicity in the following cases; dental extractions, osteoarthritis and rheumatoid arthritis (Lane, 1997; Seibert et al., 1994).

AS a continuation of our research findings on drugs (Parlak et al., 2021, 2022a, 2022b), in this work, three widely prescribed drugs and the mechanisms of their interactions when they are taken together were studied using theoretical methods. Based on the DFT calculations and QTAIM analyses, we studied their interactions. For this purpose, ESCI and IBP, ESCI and PCM couples were the targets. Their structure and activity relationship were examined based on the electronic parameters of E_{HOMO}—E_{LUMO} energies, chemical hardness (η) and electrophilicity index (ω). Furthermore, the sensitivity of ESCI to two drug molecules was also examined. Considering that $5HT_3$ and COX-2 have widely been identified as

potential targets for antidepressants (Deepali et al., 2016; Ślifirski et al., 2021) and NSAIDs (Marco & Raymond, 2002; van der Bijl & van der Bijl, 2003), respectively, we propose herein an *in silico* study of the effect of ESCI and IBP/PCM against $5HT_3$ (PDB: **6HIS**) and COX-2 (PDB: **2PXX**), respectively. Moreover, for a better understanding of the drug–drug interactions, we investigated the behavior of the mentioned drugs by docking them combined in the binding pockets of 6HIS and 2PXX, in order to evaluate the possible interactions that might link them to the targets' binding sites and thus the possibility of enhancing their effectiveness.

2. Computational studies

All the structures including ESCI, IBP and PCM were optimized in a water medium . In every step, frequency calculations were carried out as well to make sure that the obtained structures at the end of the calculations converge to a true minimum on the potential energy surfaces. In case the optimization resulted in an imaginary frequency, calculations were repeated by applying small structural changes its vibration is concerned. During the optimization processes, no geometric limitations were imposed. B3LYP (Becke, 3-parameter, Lee–Yang–Parr) functional has been widely used with acceptable results for the theoretical modeling of different types of systems (Parlak et al., 2021, 2022a, 2022b). Therefore, computational calculations were carried out at B3LYP functional along with 6-31 G(d) basis set.

The binding (E_b) or adsorption energies were calculated by using the following equation (Parlak et al., 2021, 2022a, 2022b):

$$E_b = E_{\text{Complex}} - \left[E_{\text{ESCI}} + E_{\text{Drug}} \text{ where drug is IBP or PCM}\right] \quad (1)$$

In Equation 1, E_{Complex}, E_{ESCI} and E_{Drug} are the optimized energies of the interacted complex structure, ESCI and IBP or PCM drugs correspondingly. The values of ω and η were calculated by using following relations (Parlak et al., 2021, 2022a, 2022b):

$$\omega = \mu^2/2\eta \quad (2)$$

$$\eta = [-E_{\text{HOMO}} - (-E_{\text{LUMO}})]/2 \quad (3)$$

Since all the calculations were carried out in water, the polarizable continuum model was used to observe the solvation effects (Tomasi et al., 2005). In this model water is considered as an implicit factor rather than explicit and the average dielectric effect of water is considered (Tomasi et al., 2005). In order to understand the effect of partial charge accumulations on the IR and NMR interactions at the examined sites and to make a more quantitative examination, natural bond orbital (NBO) charge analyses were also conducted (Reed et al., 1985, 1988). Since the interaction sites are close to each other, basis functions overlap and result in an error known as basis set superposition error (BSSE) causing changes in the E_b energies of the examined system (Simon et al., 1996). In this work, the BSSE errors were considered by using the counterpoise correction method. Multiwfn, GaussView and Gaussian programs were used to visualize the examined structures and for the calculations (Dennington et al., 2016; Frisch et al., 2016; Lu & Chen, 2012). Gaussian and GaussView programs were also used for the calculations and building the examined structures. The physicochemical properties and drug-likeness of investigated drugs and interactions were computed using the SwissADME website (http://swissadme.ch; Daina et al., 2017).

A molecular docking simulation with the AutoDock4.2 software and AutoDock Tools ADT (Morris et al., 2009) was performed *in silico* to investigate the interactions linking the studied drugs to their corresponding targets. X-ray crystal structures of the serotonin $5HT_3$ receptor and the cyclooxygenase enzyme COX-2 were retrieved from the RCSB protein data bank (Berman et al., 2000) with the respective PDB IDs: **6HIS** (Polovinkin et al., 2018) and **1PXX** (Rowlinson et al., 2003), which were treated by removing the co-crystallised inhibitors and co-factors. The non-polar hydrogens of the structures were merged in ADT (Morris et al., 2009) and the PDBQT format files were prepared by considering the ligands' rotatable bonds and assigning the *Gasteiger* and the *Kollman* charges to the related structures. As for the resulting docked target-drug complexes, their binding pockets were analyzed using Chimera software (Goddard et al., 2007) and Ligplot (Wallace et al., 1995) in order to evaluate the possible interacting residues.

3. Results and discussion

3.1. C≡N and OH site interactions for ESCI and IBP

The optimized structure for ESCI & IBP drug couple related to C≡N and OH site interaction is given in Figure 1. For the free single isolated IBP, the OH stretching band was calculated as 3673 cm^{-1} with an IR intensity of 159.7. Following the interaction with ESCI, the OH band of IBP showed a red-shift to a wavenumber of 3452 cm^{-1} and the IR intensity of this band increased to 1814.8. The stretching vibrational frequency of C≡N for isolated ESCI was calculated as 2338 cm^{-1} with an IR intensity of 166.6. This band was shifted slightly to the value of 2349 cm^{-1}, but the IR intensity largely shifted to 359.5. Furthermore, the OH bond length of IBP changed from 0.975 to 0.987 Å and C≡N bond length shifted slightly from 1.164 to 1.162 Å following the interaction. E_b energy for C≡N and OH site interacted system was calculated as −4.07 kcal/mol.

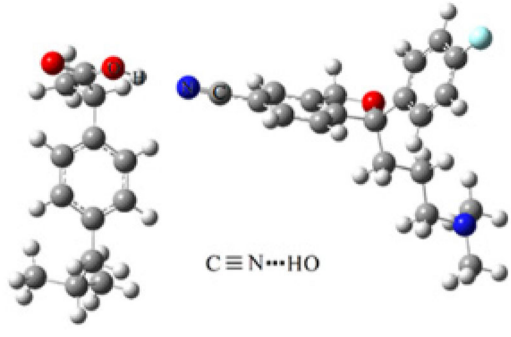

Figure 1. Optimized structure of C≡N and OH site interaction of ESCI & IBP.

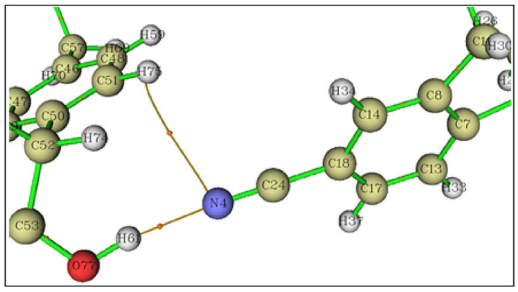

Figure 2. Molecular topographic map for C≡N and OH site interactions of ESCI & IBP.

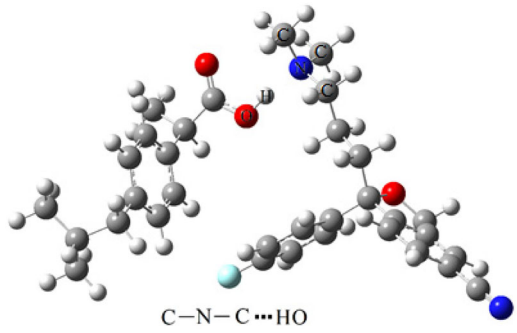

Figure 3. Optimized structure of C—N—C and OH site interaction of ESCI & IBP.

For the C≡N and OH interacted ESCI and IBP system, QTAIM results suggest two possible HB interactions, namely, O—H … N≡C and C—H … N≡C (Figure 2). For the first one, it was observed that $\nabla^2\rho > 0$ and $H < 0$ which indicate partially covalent interaction and E_{HB} was calculated as −8.02 kcal/mol. For the second one, both $\nabla^2\rho$ and H are positive indicating a non-covalent or weak interaction with E_{HB} value of −0.51 kcal/mol. The electron density at the bond critical point (BCP) for O—H … N≡C site (0.0328 a.u.) is larger than C—H … N≡C site (0.0033 a.u.) indicating stronger HB interaction for the O—H … N≡C site.

3.2. C—F and OH site interactions for ESCI and IBP

The optimized structure for ESCI & IBP drug couple for C—F and OH site interaction is given in Fig. SI1 (SI: Supplementary information). Following the interaction with the C—F site of ESCI, the vibrational OH band of IBP decreased by 18 cm^{-1} to the wavenumber of 3655 cm^{-1} and its IR intensity increased to 539.9. Stretching vibrational wavenumber of C—F for isolated ESCI was computed as 1267 cm^{-1} with IR intensity of 160.2. This band red-shifted to 1229 cm^{-1} and IR intensity slightly increased by 4.7. Furthermore, the OH bond length of IBP was nearly the same after the interaction and C—F bond length shifted from 1.354 to 1.374 Å following the interaction. E_b energy for C—F and OH site interacted system was calculated as −0.50 kcal/mol which is the smallest value for ESCI and IBP couple.

For C—F and OH interacted ESCI and IBP system, QTAIM findings proposed that three possible HB interactions occurred at O—H … F—C and C—H … F—C (ring) (Fig. SI2). For the C—F and OH site, $\nabla^2\rho > 0$, $H < 0$ indicating a partially covalent interaction with E_{HB} value of −7.53 kcal/mol. For the C—F … HC and C—H … F—C (ring) sites, both $\nabla^2\rho$ and H are positive implying non-covalent or weak interactions with E_{HB} values of −1.49 and −1.19 kcal/mol, respectively. Electron density at the BCP for O—H … F—C site was calculated as 0.0244 a.u. which is larger than C—H … F—C and C—H … F—C (ring) site interactions (0.0067 and 0.0054 a.u.) showing that the bond character is stronger for O—H … F—C site.

3.3. C–N–C and OH site interactions for ESCI and IBP

The optimized structure for ESCI & IBP drug couple for C—N—C and OH site interaction is given in Figure 3. Following the interaction with the C—N—C site of ESCI, the vibrational OH band of IBP is red-shifted from 3673 to 2499 cm^{-1} which is a remarkable change. The IR intensity also increased in a large amount from 159.7 to 4060.2. Furthermore, the OH bond length of IBP also increased from 0.975 to 1.038 Å following the interaction. Very large shifts in the vibrational wavenumbers and IR intensities of the OH group indicate that there is a very strong interaction at the C—N—C and OH sites.

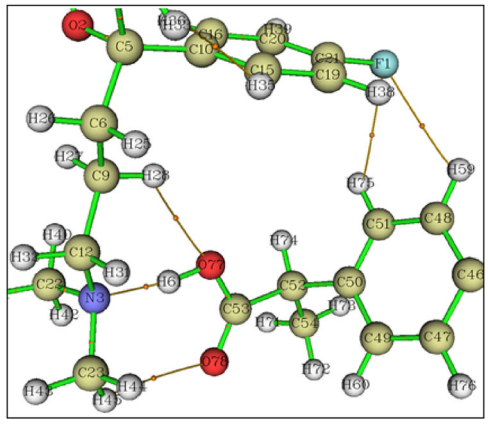

Figure 4. Molecular topographic map for C—N—C and OH site interaction of ESCI & IBP.

At this point, it is better to examine the NBO charges for three systems together. NBO charges (a.u.) given in parenthesis at the interaction site are as follows: O (−0.726) — H (+0.518) … N (−0.427)≡C, O (−0.717) — H (+0.509) … F (−0.355) and O (−0.747)—H (+0.512) … C—N (−0.530)—C. It can be seen that for C—N—C and OH site interactions, the interacting atoms are more polarized decreasing the bond character and leading to a very large red-shift in the IR spectrum. E_b energy for C—N—C and OH site interacted system was calculated as −9.75 kcal/mol which is the largest adsorption energy calculated for ESCI and IBP interacted system.

For C—N—C and OH interacted ESCI and IBP system, the results of QTAIM indicate five possible HB interactions (Figure 4). Within these five sites, O—H … N—$(C)_2$ site interaction from nitrogen atom yielded the largest E_{HB} with a value of −16.35 kcal/mol. Further, the $\nabla^2\rho > 0$ and $H < 0$ results showed that the interaction is partially covalent. The electron density at BCP was found as 0.0647 a.u. indicating a strong interaction.

3.4. HOMO–LUMO analyses for ESCI and IBP system

In general, for a given molecular system, the HOMO shows the electron-donating parts while, the LUMO indicates the electron-accepting parts (Fukui, 1982; Gunasekaran et al., 2008). HOMO–LUMO surfaces and energy values provide important information about the activity of a given molecular system (Ayala & Scuseria, 1999; Muthu & Maheswari, 2012). For the interaction occurring through accepting one electron from an enzyme, low LUMO energy value indicates a high drug activity (Behzadi et al., 2015; Bhattacharjee et al., 2002). HOMO–LUMO surfaces and the calculated E_g values for ESCI and IBP systems are given in Figures 5, SI3 and SI4.

For O—H … N≡C and O—H … F—C interacting sites, both HOMO and LUMO appear on the surface of ESCI drug molecule (Figures 5 and SI3). This fact indicates that electron acceptance and electron donation tend to occur via ESCI drug. Furthermore, following the interaction, the LUMO energy values for O—H … N≡C and O—H … F—C interacted systems become more negative as compared to single ESCI (−1.46 eV) and IBP (−0.35 eV) and this indicates a potent increase in the activity. However, this increase in activity as an electron acceptor occurs mainly on ESCI drug molecule based on the assessment of the locations of LUMOs. E_g values of single isolated ESCI and IBP were calculated as 4.33 and 6.21 eV, respectively. Furthermore, E_g values of O—H … N≡C and O—H … F—C interacted systems decreased indicating an increase in the reactivity of the interacted systems (Figures 5 and SI3).

For the O—H … N—$(C)_2$ interaction site, the HOMOs are mainly located on IBP and partially on the nitrogen moiety of ESCI (Fig. SI4). LUMOs again appear on ESCI. This fact indicates that ESCI still behaves as an electron acceptor and, IBP behaves as the main electron donor. A comparison of the E_g values of the three interacted systems shows that C≡N and OH site of interaction for ESCI and IBP produces the lowest E_g with a value of 4.13 eV, whereas C—N—C and OH site of interaction yields the highest E_g with a value of 4.82 eV.

Ionization potential (IP) may be estimated as $-E_{HOMO}$ and electron affinity (EA) is $-E_{LUMO}$ (Sylaja et al., 2018). IP and EA values for single isolated ESCI were calculated as 5.79 and 1.46 eV, respectively. Similarly, IP and EA values for IBP drug were computed as 6.56 and 0.35 eV, respectively. Among the investigated structures, C—N—C and OH interacted system produces the highest IP with a value of 6.30 eV. Among the structures examined, the highest EA value was observed with C≡N and OH site of interaction with a value of 1.66 eV.

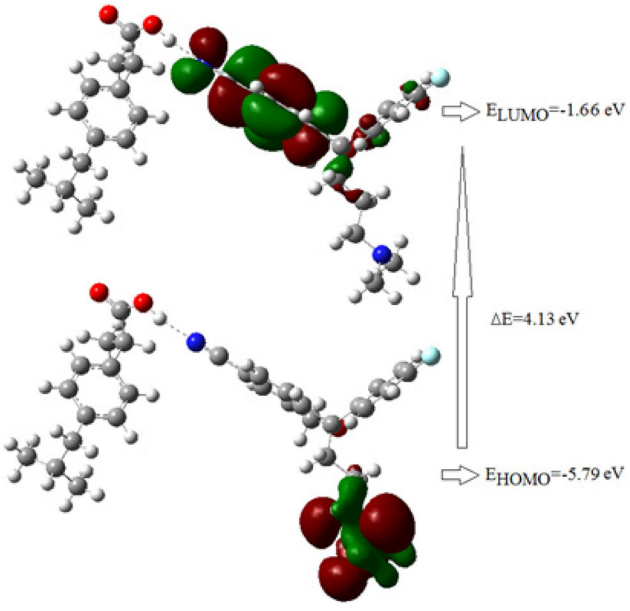

Figure 5. HOMO–LUMO distributions for C≡N and OH site interactions for ESCI and IBP.

3.5. C≡N and OH site interactions for ESCI and PCM

In the single isolated PCM the OH stretching band appears at 3739 cm^{-1} with IR intensity of 112.0. After the interaction with ESCI this band shifts to 3542 cm^{-1} with an IR intensity of 1917.1. C≡N stretching wavenumber of ESCI increased by about 10 cm^{-1} after the interaction. Moreover, the IR intensity of the C≡N stretching band increased from 166.6 to 333.8. The OH bond length of PCM increased from 0.971 to 0.981 Å, C≡N bond was slightly reduced from 1.164 to 1.162 Å following the interaction. E_b energy for C≡N and OH site interacted system was calculated as −4.18 kcal/mol (Figure 6).

QTAIM results suggest two possible HB interactions, namely O—H … N≡C and C—H … N≡C (ring) site interactions (Figure 7). For both sites, $\nabla^2\rho$ and H are positive indicating a non-covalent type of interaction. E_{HB} energies were calculated as −7.20 and −0.82 kcal/mol for O—H … N≡C and C—H … N≡C (ring) sites, respectively. Consequently, electron density at BCP for O—H … N≡C site (0.0296 a.u.) is approximately five times larger than C—H … N≡C (ring) site.

3.6. C—F and OH site interactions for ESCI and PCM

The C—F vibrational stretching of ESCI was shifted from 1267 to 1232 cm^{-1} after the interaction with the OH band of PCM (Fig. SI5). The related IR intensity also increased from 160.2 to 364.4. As a result of mutual interaction, the vibrational wavenumber of OH stretching decreased from 3739 to 3698 cm^{-1}. The related IR intensity of OH of the PCM band also increased from 112.0 to 643.9. The OH bond length of PCM was nearly the same after the interaction and the C—F bond length shifted from 1.354 to 1.371 Å after the interaction. The E_b energy for C—F and OH site interacted system

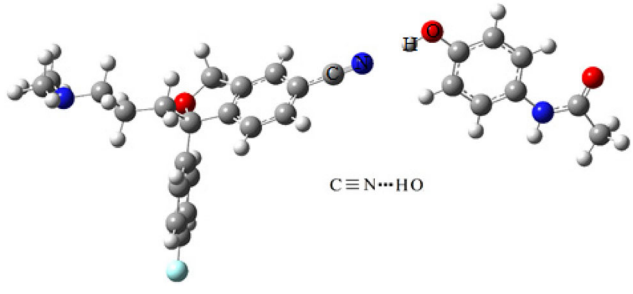

Figure 6. Optimized structure of C≡N and OH site interaction of ESCI & PCM.

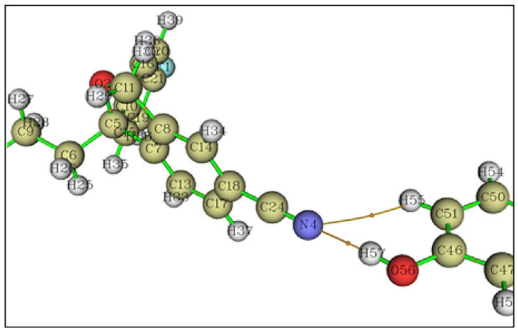

Figure 7. Molecular topographic map for C≡N and OH site interactions of ESCI & PCM.

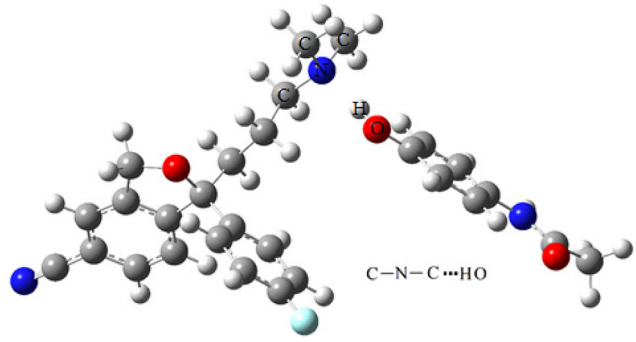

Figure 8. Optimized structure of C—N—C and OH site interaction of ESCI & PCM.

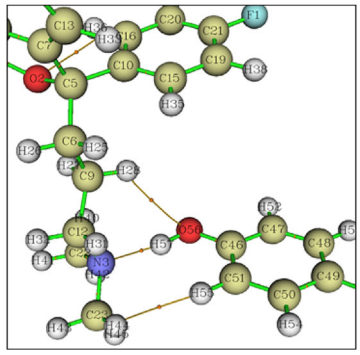

Figure 9. Molecular topographic map for C—N—C and OH site interaction of ESCI & PCM.

was calculated as −1.18 kcal/mol which was the smallest value for ESCI and PCM system.

On the basis of the QTAIM results, there are two possible HB interactions occurring at O—H … F—C and C—H … F—C (ring) sites (Fig. SI6). For the C—F and OH site, $\nabla^2\rho > 0$, $H < 0$ referring to a partially covalent interaction with E_{HB} value of −6.94 kcal/mol. As for C—H … F—C (ring) site both $\nabla^2\rho$ and H are positive which refers to a non-covalent or weak interaction with E_{HB} value of −1.42 kcal/mol.

3.7. C—N—C and OH site interactions for ESCI and PCM

After the interaction, the OH vibrational band of PCM appeared in the range of 2976–2953 cm^{-1} as combinations with CH stretching vibrations. This indicates a red-shift around between 786 and 764 cm^{-1} indicating a very strong HB interaction. The intensity of the OH band increased as well. The OH bond length of PCM also increased from 0.971 to 1.008 Å due to interaction. Since the largest vibrational shift is observed in this system, it is better to give the results of NBO charges for ESCI interacted PCM systems. The NBO charges (a.u.) given in parenthesis at the interaction site are: O (−0.725) — H (+0.511) … N (−0.423)≡C, O (−0.714) — H (+0.501) … F (−0.352) and O (−0.742) — H (+0.511) … C—N (−0.533)—C. It can be concluded that, again C—N—C and OH site interactions for ESCI and PCM couple, the interacting atoms are highly polarized causing a large red-shift in the IR spectrum. E_b energy for C—N—C and OH site interacted system (Figure 8) was calculated as −7.10 kcal/mol which is the highest adsorption energy calculated for ESCI and PCM interacted system.

For C—N—C and OH interacted ESCI and PCM system, QTAIM indicates three possible HB interactions (Figure 9). Within these interactions, the O—H … N—$(C)_2$ site interaction from nitrogen atom has the highest E_{HB} energy with a value of −11.95 kcal/mol. Further, while $\nabla^2\rho$ is positive, H was found as negative indicating a partially covalent interaction.

3.8. HOMO–LUMO analyses for ESCI and PCM system

The HOMO–LUMO surfaces and calculated values for ESCI and PCM systems are given in Figures 10, SI7 and SI8. For all of the examined ESCI and PCM combinations, while the HOMOs are located nearly all around the PCM drug molecule, the LUMOs appear on the different parts of the ESCI drug molecule (Figures 10, SI7 and SI8). This is an interesting situation and comes with possible applications. In the case of two different targets where the inhibition occurs by electron donation and electron acceptance, there could be an effective inhibition at once by using ESCI interacted PCM system since PCM possess HOMOs and ESCI has LUMO in ESCI interacted PCM drug couple. It was also found that E_g energies (3.83, 4.06 and 3.90 eV) of the ESCI&PCM couples are smaller than their constituents (5.40 and 4.33 eV) which indicates that interacted ESCI&PCM couples are more reactive than their constituents.

As indicated in previous sections, the IP and EA values for single isolated ESCI were calculated as 5.79 and 1.46 eV. IP and EA values for PCM drug were calculated as 5.60 and 0.20 eV, respectively. Among the examined drug couples, C—F and OH interacted system produced the highest IP with a value of 5.54 eV and the C—N—C and OH interacted system yielded the lowest IP with a value of 5.37 eV. Moreover, the highest EA value was observed with C≡N and OH site interactions with a value of 1.63 eV. The lowest EA value was calculated with C—N—C and OH site interactions with a value of 1.47 eV.

3.9. Physicochemical properties and drug-likeness

In this part of the study, we have examined the physicochemical characteristics and drug-likeness of the investigated drugs and drug couples. By analyzing the physicochemical properties, it is possible to obtain a global description of the structures of compounds such as molecular weight (g/mol),

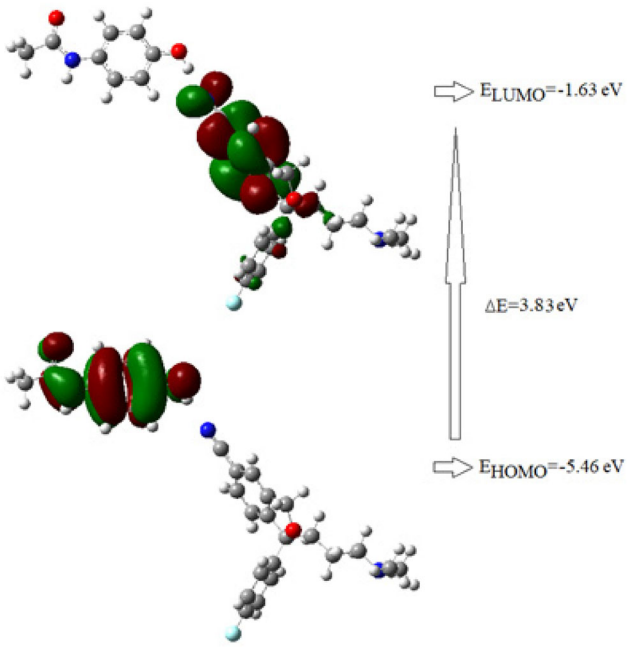

Figure 10. HOMO–LUMO distributions for C≡N and OH site interactions for ESCI and PCM.

Table 1. Physicochemical properties and lipophilicity of investigated drugs and drug couples.

Properties	ESCI	IBP	PCM	ESCI–IBP	ESCI–PCM
Molecular weight	324.39	206.28	151.16	530.67	475.55
Heavy atom	24	15	11	39	35
Arom. heavy atom	12	6	6	18	18
Fraction Csp^3	0.35	0.46	0.12	0.39	0.29
Rotatable bond	5	4	2	9	7
H-Bond acceptor	4	2	2	6	6
H-Bond donor	0	1	2	1	2
Molar refractivity	91.32	62.18	42.78	153.50	134.10
Polar surface area	36.26	37.30	49.33	73.56	85.59
Lipophilicity					
MLOGP	2.89	3.13	0.91	4.33	2.70
WLOGP	3.97	3.07	1.16	7.05	5.13
XLOGP3	3.23	3.50	0.46	4.50	3.98

molecular refractivity, topological polar surface area (Å^2), number of rotatable bonds, heavy atoms and hydrogen bond acceptors and donors (Table 1; Al Wasidi et al., 2020; Daina et al., 2017).

The bioavailability radar of the compounds makes it possible for a beforehand evaluation of drug-likeness. The bioavailability radar evaluations are based on six physicochemical properties as follows:

1. Lipophilicity (XLOGP3 between −0.7 and +5.0).
2. Size (molecular weight between 150 and 500 g/mol).
3. Polarity (the total polar surface area between 20 and 130 Å^2).
4. Solubility (log S not higher than 6).
5. Saturation (fraction Csp3 not less than 0.25).
6. Flexibility (the number of rotatable bonds is not more than 9).

The related six physicochemical properties are given in Figure 11. The pink area refers to the optimal range of the included properties and the red line shows the properties of

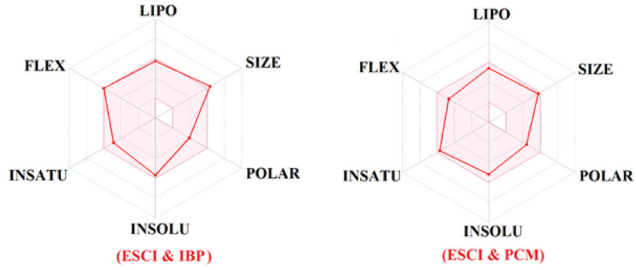

Figure 11. Bioavailability radar of the drug couples.

the compounds. In Figure 11, the red lines of combined compound ESCI–IBP are almost in the range of the pink area whereas values of the ESCI–PCM interaction are totally within the range of the pink area. Henceforth, it is possible to say that the combined drugs are predicted orally bioavailable.

Furthermore, drug-likeness was established based on the physicochemical properties to suggest oral drug candidates (Daina et al., 2017). There are five different rule-based filters that are defined as follows:

1. Lipinski's filter covers molecular weight ≤ 500, MLOGP (lipophilicity) ≤ 4.15, hydrogen bond acceptors ≤ 10, and hydrogen bond donors ≤ 5 (Lipinski et al., 2001).
2. Ghose's filter covers 160 ≤ molecular weight ≤ 480, −0.4 ≤ WLOGP (lipophilicity) ≤ 5.6, 40 ≤ the molar refractivity ≤ 130, and 20 ≤ number of atoms ≤ 70 (Ghose et al., 1999).
3. Veber's filter covers the number of rotatable bonds ≤ 10 and the total polar surface area ≤ 140 (Veber et al., 2002).
4. Egan's filter covers WLOGP (Lipophilicity) ≤ 5.88 and the total polar surface area ≤ 131 (Egan et al., 2000).
5. Muegge's filter covers 200 ≤ molecular weight ≤ 600, −2 ≤ XLOGP3 (lipophilicity) ≤ 5, the total polar surface area ≤ 150, the number of rings ≤ 7, the number of carbon > 4, the number of heteroatoms > 1, the number of rotatable bonds ≤15, the hydrogen bond acceptors ≤ 10, and the hydrogen bond donors ≤ 5 (Muegge et al., 2001).

The result of drug-likeness evaluation of the compounds is shown in Table 2. The combined ESCI–IBP structure agrees with Veber's and Muegge's rules while the combined ESCI–PCM structure agrees with all models except for Ghose's rule. The combined ESCI–PCM compound also passes all three Ghose's rules excluding one molar refractivity (MR) > 130 value. Turning to ESCI–IBP structure, it agrees with two rules of four Lipinski's rules excluding MW and MLOGP and with one rule of two Egan's rules excluding WLOGP. For four Ghose's rules, this interaction passes no one. It can be concluded that ESCI–PCM interaction is predicted orally bioavailable. Furthermore, it has better bioavailability than ESCI–IBP interaction. These preliminary results take the lead in explaining the interactions.

3.10. Molecular docking

The docking results in terms of the related decomposed energies of the most energetically favorable conformation

considered for each case of the studied protein–drug/protein–drug–codrug complex are illustrated in Table 3. The free binding energies of the complexes built of the target **6HIS** and the ligands ESCI, ESCI–IBP and ESCI–PCM were found to be −6.19, −7.13 and −8.56 kcal/mol, respectively. However, the related free binding energies obtained from docking IBP, ESCI–IBP, PCM and ESCI–PCM against the enzyme **1PXX** are −5.03, −4.10, −5.90 and −9.77 kcal/mol, respectivley.

3.11. Interactions of the drugs with 6HIS

The docking poses of the ligands ESCI, ESCI–IBP and ESCI–PCM evaluated in the docking pocket of the target **6HIS** are given in Figure 12. The ligand ESCI interacts with the binding residues of **6HIS**, namely the amino acid residues Asn_{50A} and Val_{51A}, through two N—H … O interactions of 2.77 and 3.621 Å in which ESCI acts as a hydrogen-bonding donor. In addition, this ligand forms an extra O—H … N hydrogen bond with the Tyr_{223A} residue by acting as an acceptor (Figure 13a). It is worth to be noted that the drug ESCI binds further to the **6HIS** active sites via hydrophobic interactions involving the residues Asn_{50A}, Val_{51A}, Asp_{52A}, Glu_{53A}, Lys_{54A}, Phe_{222A}, Tyr_{223A}, Ser_{270A}, Asp_{271A}, Thr_{272A}, Leu_{273A}, Pro_{274A}, Ala_{275A} and Ala_{275B} as shown in Figure 13a. Furthermore, salt-bridge interactions were observed between the drug amino group and the Asp_{52A}, Glu_{53A} amino acids.

As for the ESCI–PCM drug–codrug docked in the same target **6HIS**, the results showed that its ability to interact with the key residues of the target is enhanced since it has showed the formation of five hydrogen-bonding interactions through both its drug and co-drug, namely two N—H … N hydrogen bonds of less than 2.9 Å linking the drug ESCI to Gly_{107A} and Val_{132A}, as well as an N—H … O interaction formed between the co-drug PCM and Ile_{112A} (of 2.98 Å), in addition to a bifurcated interaction (an O—H … O and an N—H … O hydrogen bonds of 3.23 and 3.02 Å, respectively) built up with the Ser_{109A} residue (Figure 13c). Furthermore, it can be seen in Figure 13c that ESCI is involved a π–π stacking with Phe_{103A}. , Hydrophobic interactions were noticed separately around ESCI ($Asp_{97}A$, Ile_{98A}, Leu_{99A}, Phe_{103A}, Asp_{105A}, Val_{106A}, Gly_{107A}, Lys_{108A}, Ser_{109A}, Pro_{110E}, Asn_{111E}, Lys_{127A}, Gln_{130A}, Leu_{131A} and Val_{132A}) and PCM (Thr_{90A}, Lys_{108A}, Pro_{110A}, Asn_{11A}, Asn_{125A}, Lys_{127A}, Pro_{128A} and Leu_{129A}) in the ESCI–PCM case as displayed in Figure 14a. Therefore, the ESCI–PCM ligand is found to be performing better than the drug ESCI alone or the drug–drug combination ESCI–IBP docked into the binding pocket of **6HIS**, which indicates that the association of the co-drug PCM to the drug ESCI (ESCI–PCM ligand) might enhance its antidepressant-like action.

Table 2. Drug-likeness evaluation of investigated drugs and drug couples.

Rule-based filters	ESCI	IBP	PCM	ESCI–IBP	ESCI–PCM
Lipinski violations	Yes	Yes	Yes	No	Yes
Ghose violations	Yes	Yes	No	No	No
Veber violations	Yes	Yes	Yes	Yes	Yes
Egan violations	Yes	Yes	Yes	No	Yes
Muegge violations	Yes	Yes	No	Yes	Yes
Bioavailability Score	0.55	0.85	0.55	0.17	0.55

3.12. Interactions of the drugs with 1PXX

As for the complexes resulting from docking the ligands separately (IBP, PCM) or jointly with the co-drug ESCI (IBP–ESCI and PCM–ESCI) into the receptor 1PXX binding pocket are illustrated in Figure 15.

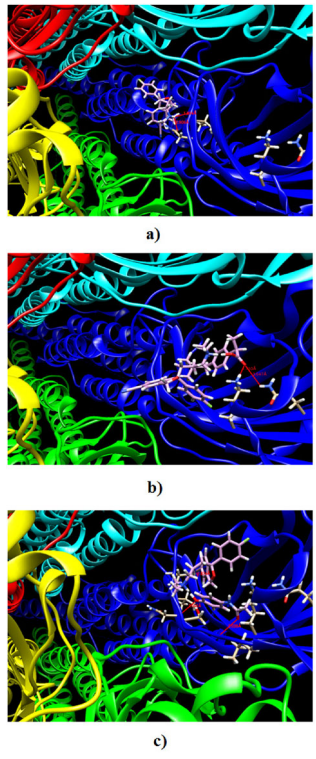

Figure 12. Docking poses of the **6HIS** target's binding sites interacting with (a) ESCI, (b) ESCI–IBP and (c) ESCI–PCM.

Table 3. Lowest free binding energies (kcal/mol) and their component terms obtained for the protein–ligand complexes.

	ΔG	$\Delta G_{vdW} + \Delta G_{Hbond} + \Delta G_{desolv}$	ΔG_{elec}	$\Delta G_{intermol}$	$\Delta G_{tot\ int}$	ΔG_{tor}	$\Delta G_{unbound}$
Ligand/receptor				6HIS			
ESCI	−6.19	−6.43	−1.25	−7.68	−1.19	+1.49	−1.19
ESCI–IBP	−7.13	−9.29	−1.41	−10.71	−3.51	+3.58	−3.51
ESCI–PCM	−8.56	−11.08	−0.17	−11.25	−2.29	+2.68	−2.29
				1PXX			
IBP	−5.03	−5.41	−1.11	−6.52	−0.41	+1.49	−0.41
ESCI–IBP	−4.10	−7.15	+0.06	−7.08	−3.32	+2.98	−3.32
PCM	−5.90	−6.40	−0.10	−6.49	−0.17	+0.60	−0.17
ESCI–PCM	−9.77	−12.08	+0.22	−11.86	−1.53	+2.09	−1.53

Where ΔG is the binding affinity, $\Delta G_{intermol}$ is the final intermolecular energy ($\Delta G_{vdW} + \Delta G_{Hbond} + \Delta G_{desolv} + \Delta G_{elec}$), $\Delta G_{tot\ int}$ is the final total internal energy, ΔG_{tor} is the torsional free energy and $\Delta G_{unbound}$ is the unbound system's energy.

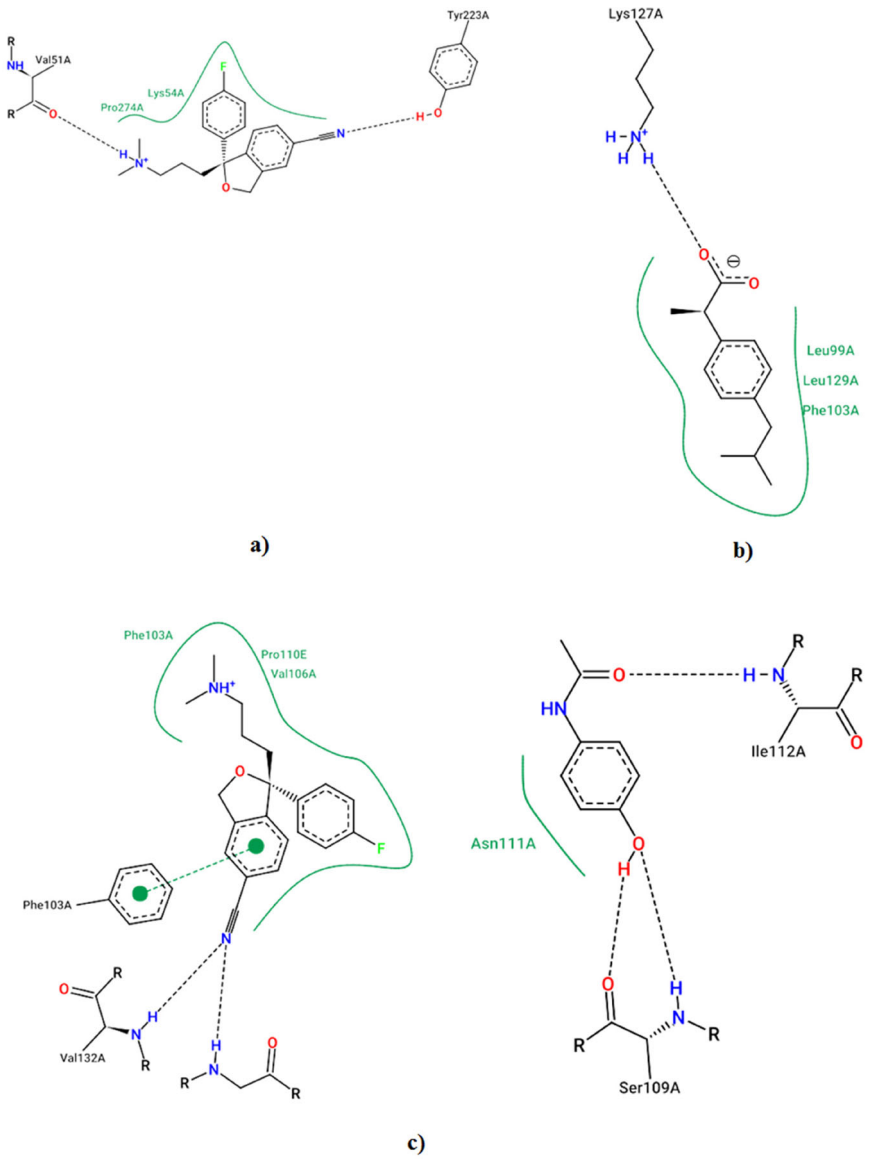

Figure 13. Hydrogen bonds formed between **6HIS** and (a) ESCI, (b) ESCI–IBP, (c) ESCI–PCM. For the sake of clarity, the binding pockets involving the drug–drug combination were split in each case (Fricker et al., 2004; Stierand et al., 2006).

We have noticed that the ligand IBP displays three hydrogen bonds, namely an N—H … O (of 3.03 Å) and two O—H … O (of 2.82 and 3.30 Å) resulting from the residues Lys_{342A}, Asn_{560A} and Phe_{361A} respectively (Figure 16a). Furthermore, two extra N—H … O (Figure 16a) and O—H … O (Figure 17a) interactions link the ligand to the amino acid Asn_{560A}, as well as hydrophobic interactions, depicted in Figure 17a as red arcs with spokes radiating towards the ligand atoms they connect to while the contacted atoms are drawn with spokes radiating back, and resulting from Glu_{346A}, Lys_{360A}, Asp_{362A}, Pro_{363A}, Glu_{364A}, Trp_{545A} and Phe_{556A} (Figure 17a). When combined with the co-drug ESCI, the drug IBP shows less hydrogen bonding interactions and interacts with **1PXX** through only two O—H … O H-bonds resulting from Ser_{530A} and Tyr_{385A} (Figure 16b). Whereas, the co-drug ESCI shows a long N—H … F interaction of 3.5 Å (Figure 17b), in which it acts as an acceptor. İt is worth to be noted that both drugs combined share the same surrounding hydrophobic contacts obtained among others from the residues Val_{116A}, Val_{349A}, Leu_{352A}, Leu_{359A}, Phe_{381A}, Tyr_{385A}, Gly_{526A}, Ala_{527A} and Leu_{531A} (Figure 17b). Thus, the anti-inflammatory potential of the drug IBP did not improve much while combined with the co-drug ESCI (ESCI–IBP ligand) even though it has interacted with amino acid residues in the binding pocket of **1PXX**.

As for the ligand PCM, it presents two H-bonds (Figure 15c) one of each type N—H … O (Ser_{530A}: 2.80 Å) and O—H … O (Asn_{375A}: 3.15 Å). Two additional long N—H … O interactions are built up between the ligand and the Val_{228A} and Ser_{530A} amino acids (Figure 17c). Furthermore, the ligand shows a $\pi \ldots \pi$ stacking linking its ring to the Phe_{209A} residue and displays hydrophobic interactions with Phe_{205A}, Thr_{206A}, Phe_{209A}, His_{226A}, Gly_{227A}, Val_{344A}, Tyr_{348A}, Ile_{377A}, Phe_{381A}, Tyr_{385A}, Phe_{529A}, Gly_{533A} and Leu_{534A}. However, PCM has showed one N—H … O H-Bond in **1PXX** binding pocket through the Val_{116A} amino acid after its association with the co-drug ESCI (Figure 16d). The co-drug ESCI in the ESCI–PCM case binds to the

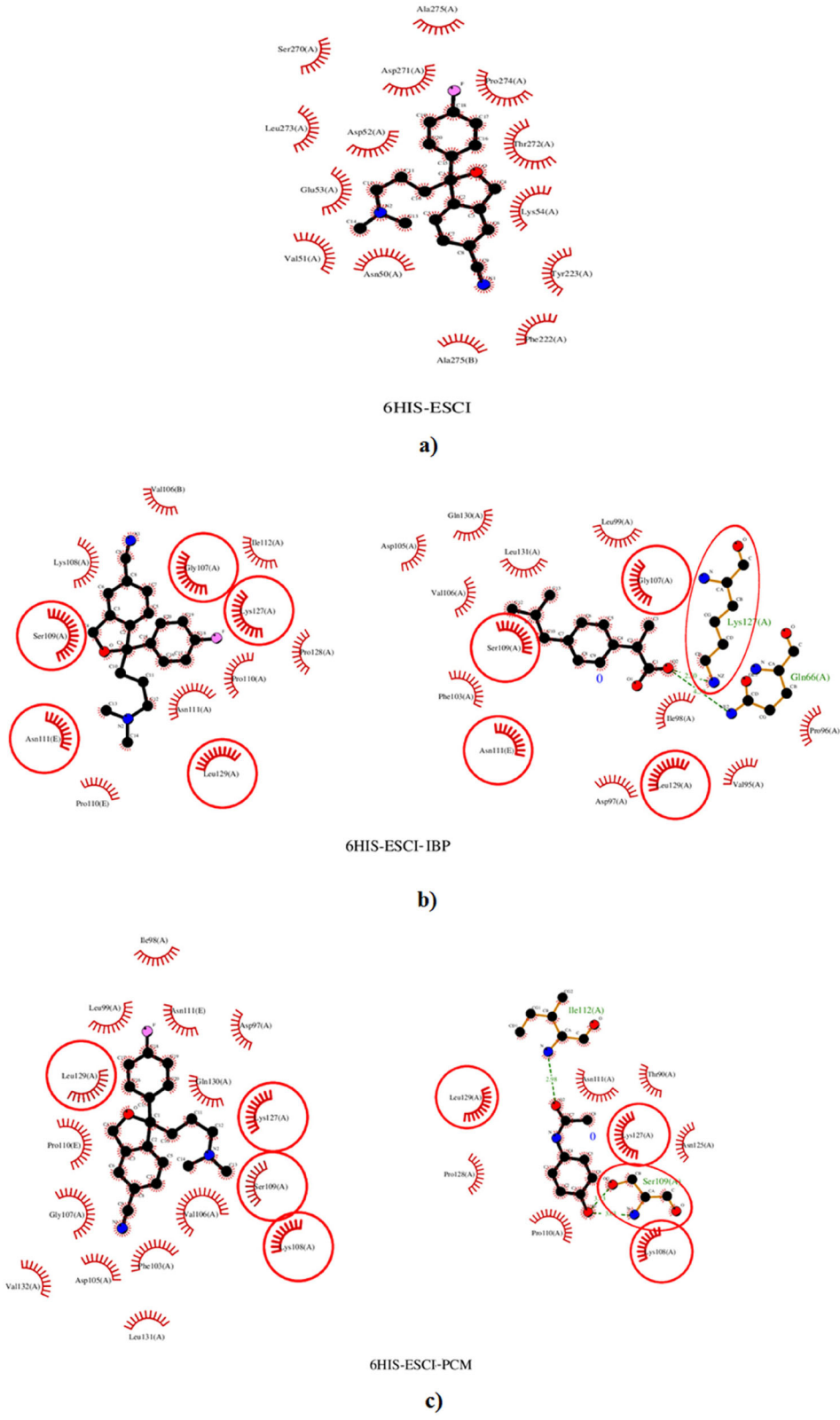

Figure 14. Hydrophobic interactions linking **6HIS** to (a) ESCI, (b) ESCI–IBP and (c) ESCI–PCM. Hydrogen bonds are depicted as dashed lines and hydrophobic contacts as arcs.

active sites of **1PXX** *via* two N—H … F interactions of 2.64 and 3.97 Å (Figure 17d). Whereas, both PCM and ESCI share the hydrophobic interactions formed with Val_{116A}, Tyr_{355A}, Leu_{359A}, Ala_{527A} and Leu_{531A}. Therefore, by interacting with the **1PXX** target's active sites the association of ESCI to PCM (ESCI–PCM ligand) could be considered as potent as the use of PCM alone as an analgesic and anti-inflammatory drug.

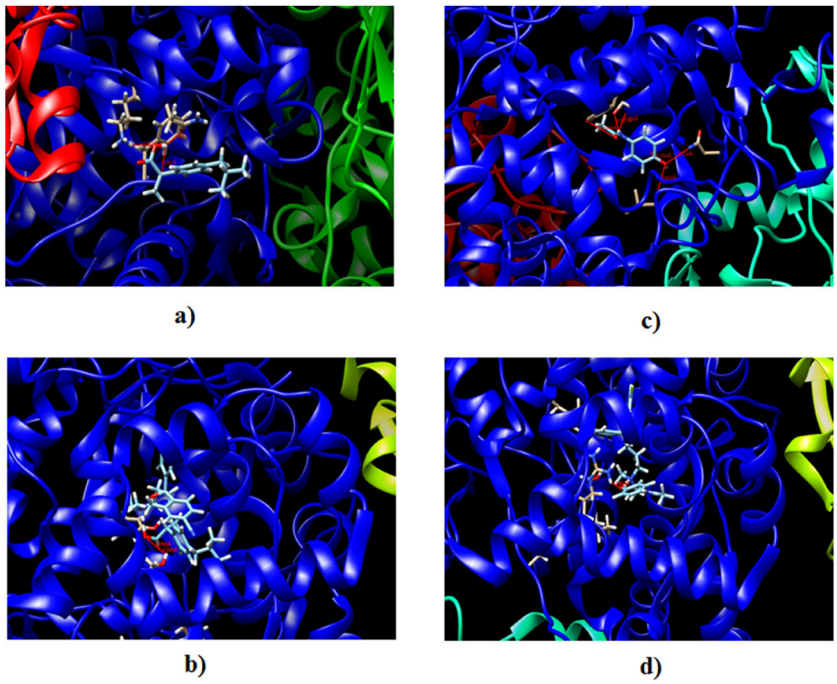

Figure 15. Best poses of (a) IBP, (b) ESCI–IBP, (c) PCM and (d) ESCI–PCM docked into the binding pocket of **1PXX**.

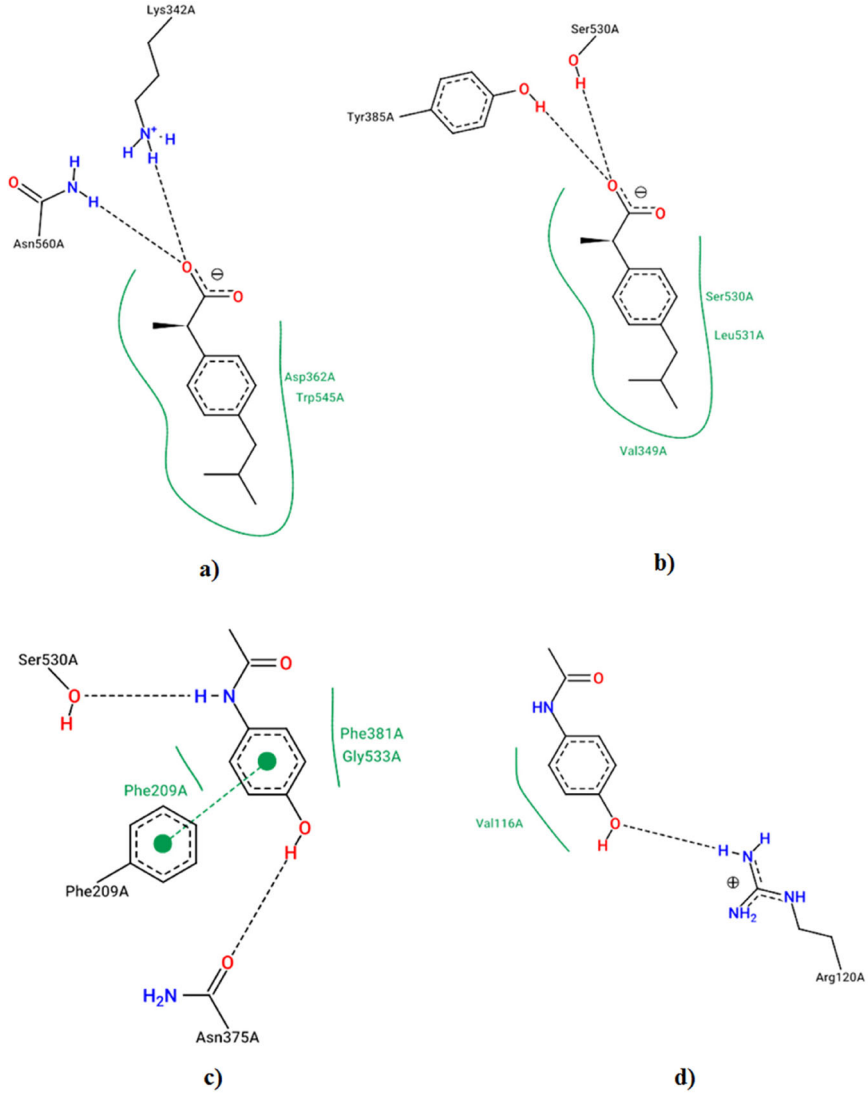

Figure 16. Hydrogen bonds observed in the binding pocket of **1PXX** linking it to the ligands (a) IBP, (b) ESCI–IBP, (c) PCM and (d) ESCI–PCM.

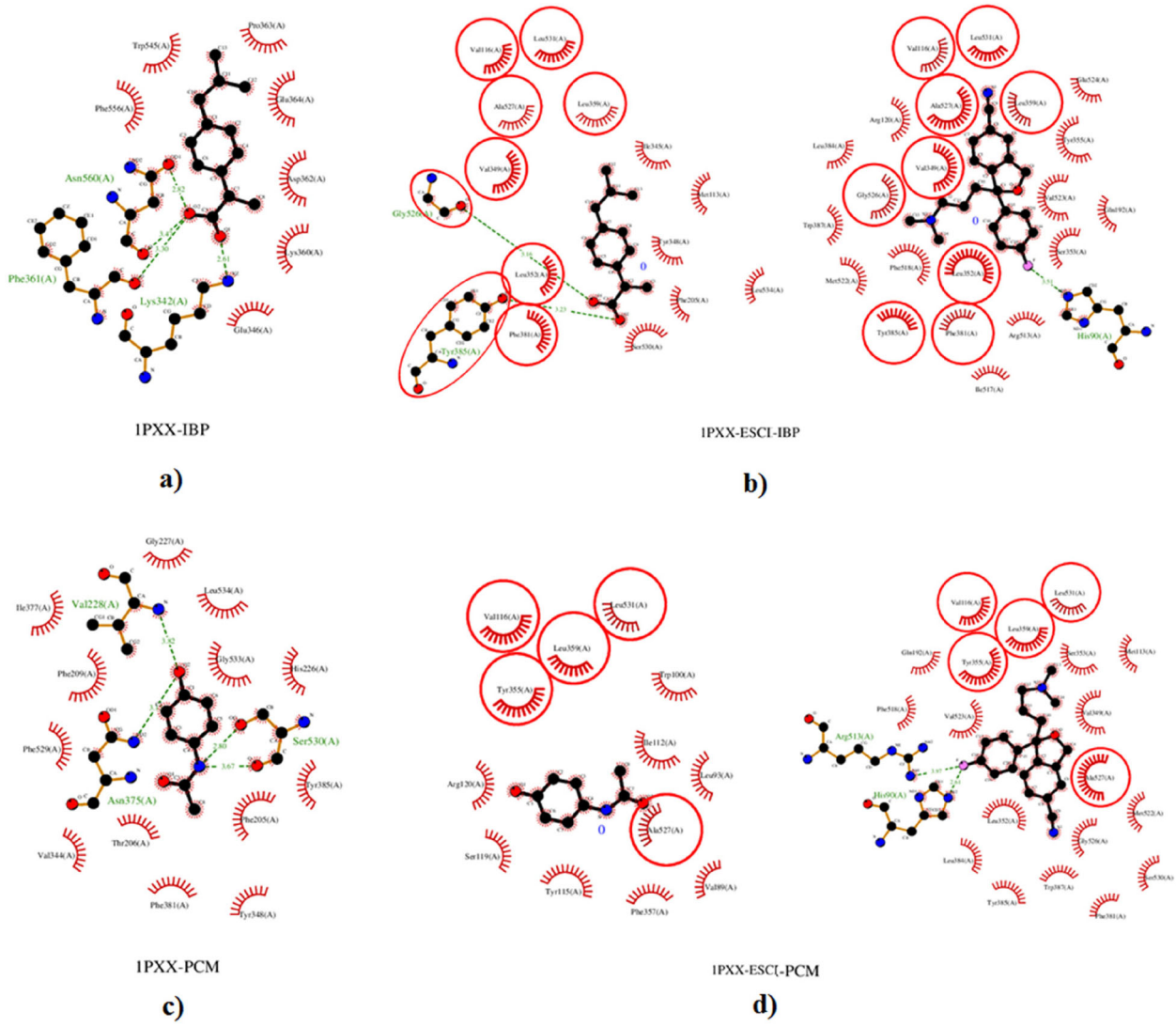

Figure 17. Hydrophobic contacts and hydrogen bonds observed between **1PXX** and (a) IBP, (b) ESCI–IBP, (c) PCM, (d) ESCI–PCM. Hydrogen bonds are depicted as dashed lines and hydrophobic contacts as arcs.

4. Conclusions

In this study, the structure and activity relationship of ESCI, IBP and PCM drug couples were examined based on DFT calculations. In summary, the following conclusions were reached:

i. The interaction between ESCI with IBP and PCM drugs can be monitored from the changes of vibrational wavenumbers where the interaction occurs.
ii. O—H … N—$(C)_2$ site interacted system for ESCI–IBP and ESCI–PCM was the most stable structure whereas O—H … N≡C interacting site was found to be more reactive than others.
iii. The charge transfer in the interactions was from IBP or PCM to ESCI. Chemical reactivity of each drug couple increased compared to their constituents based on the HOMO–LUMO energy gap assessments. Energy gaps were decreased upon interaction. ESCI and IBP drug couples were found more reactive compared to ESCI and IBP drug couples.
iv. It was observed that HOMO–LUMO distributions showed dependency where the interaction takes place between the drug molecules. For each interaction examined in this work, LUMOs are located on the ESCI drug molecule with a more negative LUMO energy value. Therefore, in the cases where the interaction mechanism occurs via accepting one electron an enzyme the activity of ESCI tends to increase upon interaction. The degree and effect of this increase can be subject of another study.
v. ESCI and PCM couple system fulfils all requirements of Lipinski, Veber, Egan and Muegge rules except for Ghose's rule and it has better bioavailability than ESCI–IBP couple.
vi. By carrying out an *in silico* study of the ligands against **6HIS**; namely the separate drug ESCI as well as the combined drugs ESCI–PCM and ESCI–IBP, we have found that the ESCI–PCM association performed better than the drug ESCI alone or the other drug combination (ESCI–IBP), in terms of the formation of N—H … N, O—H … O and N—H … O hydrogen bonds,

hydrophobic interactions and π-π stacking built up with the target, which indicates that this association might enhance the ESCI antidepressant-like action.

vii. In the case of **1PXX**, after docking the ligands separately (IBP, PCM) and jointly with the co-drug ESCI (IBP–ESCI, PCM–ESCI) into the target's binding pocket, it turned out that the anti-inflammatory potential of the drug IBP did not improve after combining with ESCI (ESCI–IBP). However , the association of ESCI with PCM (ESCI–PCM) is as potent as PCM alone, and thus could be considered as an effective analgesic and anti-inflammatory drug combination.

Disclosure statement

No potential conflict of interest was reported by the author(s).

Funding

Authors acknowledge Fencluster system of Ege University for the calculations. This work was supported by Ege University Scientific Research Projects Coordination Unit (Project Number: FHD_2021_22880). AD would like to acknowledge the fund of the Ministry of Higher Education and Research Sciences MESRS and Abbes Laghrour University of Khenchela (Algeria) under the Project Number: B00L01UN400120210002 (PRFU).

References

Thun, M. J., Namboodiri, M. M., & Heath, C. W. Jr (1991). Aspirin use and reduced risk of fatal colon cancer. *The New England Journal of Medicine*, *325*(23), 1593–1596. https://doi.org/10.1056/NEJM199112053252301

Al Wasidi, A. S., Hassan, A. S., & Naglah, A. M. (2020). In vitro cytotoxicity and druglikeness of pyrazolines and pyridines bearing benzofuran moiety. *Journal of Applied Pharmaceutical Science*, *10*, 142–148.

Anderson, B. J. (2008). Paracetamol (acetaminophen): mechanisms of action, Paediatr. *Paediatric Anaesthesia*, *18*(10), 915–921. https://doi.org/10.1111/j.1460-9592.2008.02764.x

Ayala, P. Y., & Scuseria, G. E. (1999). Linear scaling second-order Moller–Plesset theory in the atomic orbital basis for large molecular systems. *Journal of Chemical Physics*. *110*(8), 3660–3671. https://doi.org/10.1063/1.478256

Bader, R. F. W. (1990). *In atoms in molecules: A quantum theory*. Clarendon Press.

Bang-Andersen, B., Ruhland, T., Jørgensen, M., Smith, G., Frederiksen, K., Jensen, K. G., Zhong, H., Nielsen, S. M., Hogg, S., Mørk, A., & Stensbøl, T. B. (2011). Discovery of 1-[2-(2,4-dimethylphenylsulfanyl)phenyl]piperazine (Lu AA21004): A novel multimodal compound for the treatment of major depressive disorder. *Journal of Medicinal Chemistry*, *54*(9), 3206–3221. https://doi.org/10.1021/jm101459g

Barone, V. (Ed.) (2011). *Computational strategies for spectroscopy, from small molecules to nano systems*. John Wiley & Sons, Inc.

Behzadi, H., Roonasi, P., Taghipou, K. A., van der Spoel, D., & Manzetti, S. (2015). Relationship between electronic properties and drug activity of seven quinoxaline compounds: A DFT study. *Journal of Molecular Structure*, *1091*, 196–202. https://doi.org/10.1016/j.molstruc.2015.03.001

Berman, H. M., Westbrook, J., Feng, Z., Gilliland, G., Bhat, T. N., Weissig, H., Shindyalov, IN., & Bourne, P. E. (2000). The Protein Data Bank. *Nucleic Acids Research*, *28*(1), 235–242. https://doi.org/10.1093/nar/28.1.235

Bhattacharjee, A. K., Skanchy, D. J., Jennings, B., Hudson, T. H., Brendle, J. J., & Werbovetz, K. A. (2002). Analysis of stereoelectronic properties, mechanism of action and pharmacophore of synthetic ındolo[2,1-b]quinazoline-6,12-dione derivatives in relation to antileishmanial activity using quantum chemical, cyclic voltammetry and 3-D-QSAR catalyst procedures. *Bioorganic & Medicinal Chemistry*, *10*(6), 1979–1989. https://doi.org/10.1016/S0968-0896(02)00013-5

Cao, M., Wu, D., Yoosefian, M., Sabaei, S., & Jahani, M. (2020). Comprehensive study of the encapsulation of Lomustine anticancer drug into single walled carbon nanotubes (SWCNTs): Solvent effects, molecular conformations, electronic properties and intramolecular hydrogen bond strength. *Journal of Molecular Liquids*, *320*, 114285. https://doi.org/10.1016/j.molliq.2020.114285

Chan, G., Boyle, J. O., Yang, E. K., Zhang, F., Sacks, P. G., Shah, J. P., Edelstein, D., Soslow, R. A., Koki, A. T., Woerner, B. M., Masferrer, J. L., & Dannenberg, A. J. (1999). Cyclooxygenase-2 expression is up-regulated in squamous cell carcinoma of the head and neck. *Cancer Research*, *59*(5), 991–994.,

Chey, W. D., Kurlander, J., & Eswaran, S. (2015). Irritable bowel syndrome: A clinical review. *JAMA*, *313*(9), 949–958. https://doi.org/10.1001/jama.2015.0954

Daina, A., Michielin, O., & Zoete, V. (2017). SwissADME: A free web tool to evaluate pharmacokinetics, drug-likeness and medicinal chemistry friendliness of small molecules. *Scientific Reports*, *7*, 42717. https://doi.org/10.1038/srep42717

Deepali, G., Visakh, P., & Mahesh, R. (2016). 5HT3 receptors: Target for new antidepressant drugs. *Neuroscience & Biobehavioral Reviews*, *64*, 311–325.

Dennington, R. D., Keith, T. A., & Millam, J. M. (2016). *GaussView 6.0.16*. Gaussian Inc.

Derry, C. J., Derry, S., & Moore, R. A. (2013). Single dose oral ibuprofen plus paracetamol (acetaminophen) for acute postoperative pain. *Cochrane Database Systematic Reviews*, *6*, 1–31.

Dhillon, S., Scott, L. J., & Plosker, G. L. (2006). Escitalopram a review of its use in the management of anxiety disorders. *CNS Drugs*, *20*(9), 763–790. https://doi.org/10.2165/00023210-200620090-00010

Doherty, M., Hawkey, C., Goulder, M., Gibb, I., Hill, N., Aspley, S., & Reader, S. (2011). A randomised controlled trial of ibuprofen, paracetamol or a combination tablet of ibuprofen/paracetamol in community-derived people with knee pain. *Annals of the Rheumatic Diseases*, *70*(9), 1534–1541. https://doi.org/10.1136/ard.2011.154047

Eberhart, C. E., Coffey, R. J., Radhika, A., Giardiello, F. M., Ferrenbach, S., & DuBois, R. N. (1994). Up-regulation of cyclooxygenase-2 gene expression in human colorectal adenomas and adenocarcinomas. *Gastroenterology*, *107*(4), 1183–1188. https://doi.org/10.1016/0016-5085(94)90246-1

Eccles, R., Holbrook, A., & Jawad, M. (2010). A double-blind, randomised, crossover study of two doses of a single-tablet combination of ibuprofen/paracetamol and placebo for primary dysmenorrhea. *Current Medical Research and Opinion*, *26*(11), 2689–2699. https://doi.org/10.1185/03007995.2010.525028

Egan, W. J., Merz, K. M., & Baldwin, J. J. (2000). Prediction of drug absorption using multivariate statistics. *Journal of Medicinal Chemistry*, *43*(21), 3867–3877. https://doi.org/10.1021/jm000292e

Fakhfouri, G., Rahimian, R., Dyhrfjeld-Johnsen, J., Zirak, M. R., & Beaulieu, J.-M. (2019). 5-HT3 receptor antagonists in neurologic and neuropsychiatric disorders: The iceberg still lies beneath the surface. *Pharmacological Reviews*, *71*(3), 383–412. https://doi.org/10.1124/pr.118.015487

Flynn, E. (2007). Drug-drug interactions, xPharm: The Comprehensive Pharmacology Reference. 1–3.

Fornaro, T., Burini, D., Biczysko, M., & Barone, V. (2015). Hydrogen-bonding effects on ınfrared spectra from anharmonic computations: uracil − water complexes and uracil dimers. *The Journal of Physical Chemistry. A*, *119*(18), 4224–4236. https://doi.org/10.1021/acs.jpca.5b01561

Fricker, P. C., Gastreich, M., & Rarey, M. (2004). Automated drawing of structural molecular formulas under constraints. *Journal of Chemical İnformation and Computer Sciences*, *44*(3), 1065–1078. https://doi.org/10.1021/ci049958u

Frisch, M. J., Trucks, G. W., & Schlegel, H. B. (2016). *Gaussian 16, Revision C.01*. Gaussian Inc.

Fukui, K. (1982). Role of frontier orbitals in chemical reactions. *Science (New York, N.Y.)*, *218*(4574), 747–754. https://doi.org/10.1126/science.218.4574.747

Gandhi, J., Khera, L., Gaur, N., Paul, C., & Kaul, R. (2017). Role of modulator of ınflammation cyclooxygenase-2 in gammaherpesvirus mediated tumorigenesis. *Frontiers in Microbiology*, *8*, 538. https://doi.org/10.3389/fmicb.2017.00538

Ghose, A. K., Viswanadhan, V. N., & Wendoloski, J. J. (1999). A knowledge-based approach in designing combinatorial or medicinal chemistry libraries for drug discovery. 1. A qualitative and quantitative characterization of known drug databases. *Journal of Combinatorial Chemistry*, *1*(1), 55–68. https://doi.org/10.1021/cc9800071

Giovannucci, E., Rimm, E. B., Stampfer, M. J., Colditz, G. A., Ascherio, A., & Willett, W. C. (1994). Aspirin use and the risk for colorectal cancer and adenoma in male health professionals. *Annals of İnternal Medicine*, *121*(4), 241–246. https://doi.org/10.7326/0003-4819-121-4-199408150-00001

Goddard, T. D., Huang, C. C., & Ferrin, T. E. (2007). Visualizing density maps with UCSF Chimera. *Journal of Structural Biology*, *157*(1), 281–287. https://doi.org/10.1016/j.jsb.2006.06.010

Grabowski, S. J. (2011). What ıs the covalency of hydrogen bonding? *Chemical Reviews*, *111*(4), 2597–2625. https://doi.org/10.1021/cr800346f

Gunasekaran, S., Balaji, R. A., Kumeresan, S., Anand, G., & Srinivasan, S. (2008). Experimental and theoretical investigations of spectroscopic properties of N-acetyl-5-methoxytryptamine. *Canadian Journal of Analytical Sciences and Spectroscopy*, *53*, 149–162.

Hida, T., Yatabe, Y., Achiwa, H., Muramatsu, H., Kozaki, K., Nakamura, S., Ogawa, M., Mitsudomi, T., Sugiura, T., & Takahashi, T. (1998). Increased expression of cyclooxygenase-2 occurs frequently in human lung cancer, specifically in adenocarcinomas. *Cancer Research*, *58*(17), 3761–3764.

Hirano, Y., Takeda, K., & Miki, K. (2016). Charge-density analysis of an iron–sulfur protein at an ultra-high resolution of 0.48 Å. *Nature*, *534*(7606), 281–284. https://doi.org/10.1038/nature18001

Hohenberg, P., & Kohn, W. (1964). Inhomogeneous electron gas. *Physical Review*, *136*(3B), B864–B871. https://doi.org/10.1103/PhysRev.136.B864

Hoozemans, J. J., Veerhuis, R., Rozemuller, A. J., & Eikelenboom, P. (2003). Non-steroidal anti-inflammatory drugs and cyclooxygenase in Alzheimer's disease. *Current Drug Targets*, *4*(6), 461–468. https://doi.org/10.2174/1389450033490902

Jensen, P., & Bunker, P. R. (2000). *Computational molecular spectroscopy*. John Wiley and Sons Ltd.

Jonathan, R. T., Davidson, M. D., Bose, A., Korotzer, A., & Zheng, H. (2004). Escitalopram in the treatment of generalized anxiety disorder: Double-blind, placebo controlled, flexible-dose study. *Depression and Anxiety*, *19*(4), 234–240. https://doi.org/10.1002/da.10146

Kargman, S. L., O'Neill, G. P., Vickers, P. J., Evans, J. F., Mancini, J. A., & Jothy, S. (1995). Expression of prostaglandin G/H synthase-1 and -2 protein in human colon cancer. *Cancer Research*, *55*, 2556–2559.

Kawakami, J., Kakinami, H., Matsushima, N., Nakane, A., Kitahara, H., Nagaki, M., & Ito, S. (2013). Structure—activity relationship analysis for antimicrobial activities of tryptanthrin derivatives using quantum chemical calculation. *Journal of Computer Chemistry, Japan*, *12*(2), 109–112. https://doi.org/10.2477/jccj.2012-0026

Kraka, E., & Cremer, D. (2000). Computer design of anticancer drugs. A new enediyne warhead. *Journal of the American Chemical Society*, *122*(34), 8245–8264. https://doi.org/10.1021/ja001017k

Lane, N. E. (1997). Pain management in osteoarthritis: The role of COX-2 inhibitors. *Journal of Rheumatology*, *24*, 20–24.

Langhendries, J. P., Allegaert, K., Van Den Anker, J. N., Veyckemans, F., & Smets, F. (2016). Possible effects of repeated exposure to ibuprofen and acetaminophen on the intestinal immune response in young infants. *Medical Hypotheses*, *87*, 90–96. https://doi.org/10.1016/j.mehy.2015.11.012

Lazarević, J. J., Uskoković-Marković, S., Jelikić-Stankov, M., Radonjić, M., Tanasković, D., Lazarević, N., & Popović, Z. V. (2014). Intermolecular and low-frequency intramolecular Raman scattering study of racemic ibuprofen. *Spectrochimica Acta. Part A, Molecular and Biomolecular Spectroscopy*, *126*, 301–305.) https://doi.org/10.1016/j.saa.2014.01.135

Lipinski, C. A., Lombardo, F., Dominy, B. W., & Feeney, P. J. (2001). Experimental and computational approaches to estimate solubility in drug discovery and development settings. *Advanced Drug Delivery Reviews*, *46*(1–3), 3–26. https://doi.org/10.1016/s0169-409x(00)00129-0

Lu, T., & Chen, F. (2012). Multiwfn: A multifunctional wavefunction analyser. *Journal of Computational Chemistry*, *33*(5), 580–592. https://doi.org/10.1002/jcc.22885

Marco, E. T., & Raymond, N. D. (2002). Cyclooxygenase-2: A therapeutic target. *Review Annu. Rev. Med*, *53*, 35–57.

McGeer, P. L. (2000). Cyclo-oxygenase-2 inhibitors: Rationale and therapeutic potential for Alzheimer's disease. *Drugs & Aging*, *17*(1), 1–11. https://doi.org/10.2165/00002512-200017010-00001

Mehdipour, A. R., Safarpour, A. M., Taghavi, F., & Jamali, M. (2009). Density functional theory-based quantitative structure activity relationship (QSAR) study of alkanol and alkanthiol derivatives. *QSAR & Combinatorial Science*, *28*(5), 568–575. https://doi.org/10.1002/qsar.200860124

Mirhaji, E., Afshar, M., Rezvani, S., & Yoosefian, M. (2018). Boron nitride nanotubes as a nanotransporter for anti-cancer docetaxel drug in water/ethanol solution. *Journal of Molecular Liquids*, *271*, 151–156. https://doi.org/10.1016/j.molliq.2018.08.142

Morris, G. M., Huey, R., Lindstrom, W., Sanner, M. F., Belew, R. K., Goodsell, D. S., & Olson, A. J. (2009). Autodock4 and AutoDockTools4: Automated docking with selective receptor flexiblity. *Journal of Computational Chemistry*, *30*(16), 2785–2791. https://doi.org/10.1002/jcc.21256

Muegge, I., Heald, S. L., & Brittelli, D. (2001). Simple selection criteria for drug-like chemical matter. *Journal of Medicinal Chemistry*, *44*(12), 1841–1846. https://doi.org/10.1021/jm015507e

Muthu, S., & Maheswari, J. U. (2012). Quantum mechanical study and spectroscopic (FT-IR, FT-Raman, 13C, 1H, UV) study, first order hyperpolarizability, NBO analysis, HOMO and LUMO analysis of 4-[(4-aminobenzene) sulfonyl] aniline by ab initio HF and density functional method. *Spectrochimica Acta. Part A, Molecular and Biomolecular Spectroscopy*, *92*, 154–163. https://doi.org/10.1016/j.saa.2012.02.056

Najafi, M., Morsali, A., & Bozorgmehr, M. R. (2019). DFT study of SiO_2 nanoparticles as a drug delivery system: Structural and mechanistic aspects. *Structural Chemistry*, *30*(3), 715–726. https://doi.org/10.1007/s11224-018-1227-9

Nemecz, À., Prevost, M. S., Menny, A., & Corringer, P.-J. (2016). Emerging molecular mechanisms of signal transduction in pentameric ligand-gated ion channels. *Neuron*, *90*(3), 452–470. https://doi.org/10.1016/j.neuron.2016.03.032

Oh, C.-M., Namkung, J., Go, Y., Shong, K. E., Kim, K., Kim, H., Park, B.-Y., Lee, H. W., Jeon, Y. H., Song, J., Shong, M., Yadav, V. K., Karsenty, G., Kajimura, S., Lee, I. K., Park, S., & Kim, H. (2015). Regulation of systemic energy homeostasis by serotonin in adipose tissues. *Nature Communications*, *6*, 6794. https://doi.org/10.1038/ncomms7794

Owens, M. J., Knight, D. L., & Nemeroff, C. B. (2001). Second-generation SSRIs:human monoamine transporter binding profile of escitalopram and R-fluoxetine. *Biological Psychiatry*, *50*(5), 345–350. https://doi.org/10.1016/s0006-3223(01)01145-3

Parlak, C., Alver, Ö., & Bağlayan, Ö. (2021). Quantum mechanical simulation of Molnupiravir drug interaction with Si-doped C-60 fullerene. *Computational and Theoretical Chemistry*, *1202*, 113336. https://doi.org/10.1016/j.comptc.2021.113336

Parlak, C., Alver, Ö., Ouma, C. N. M., Rhyman, L., & Ramasami, P. (2022a). Can the antivirals remdesivir and favipiravir work better jointly? In silico ınsights. *Drug Research*, *72*(1), 34–40. https://doi.org/10.1055/a-1585-1323

Parlak, C., Alver, Ö., Ouma, C. N. M., Rhyman, L., & Ramasami, P. (2022b). Interaction between favipiravir and hydroxychloroquine and their combined drug assessment: İn silico investigations. *Chemicke Zvesti*, *76*(3), 1471–1478. https://doi.org/10.1007/s11696-021-01946-8

Parrett, M. L., Harris, R., Joarder, F. S., Ross, M. S., Clausen, K. P., & Robertson, F. M. (1997). Cyclooxygenase-2 gene expression in human breast cancer. *International Journal of Oncology*, *10*(3), 503–507. https://doi.org/10.3892/ijo.10.3.503

Parthasarathi, R., Amutha, R., Subramanian, V., Nair, B. U., & Ramasami, T. (2004). Bader's and reactivity descriptors' analysis of DNA base pairs. *The Journal of Physical Chemistry A*, *108*(17), 3817–3828. https://doi.org/10.1021/jp031285f

Parthasarathi, R., Subramanian, V., & Sathyamurthy, N. (2005). Hydrogen bonding in phenol, water, and phenol − water clusters. *The Journal of Physical Chemistry. A*, *109*(5), 843–850. https://doi.org/10.1021/jp046499r

Paulino, M., Alvareda, E. M., Denis, P. A., Barreiro, E. J., Sperandio da Silva, G. M., Dubin, M., Gastellú, C., Aguilera, S., & Tapia, O. (2008). Studies of trypanocidal (inhibitory) power of naphthoquinones: Evaluation of quantum chemical molecular descriptors for structure activity relationships. *European Journal of Medicinal Chemistry*, *43*(10), 2238–2246. https://doi.org/10.1016/j.ejmech.2007.12.023

Polovinkin, L., Hassaine, G., Perot, J., Neumann, E., Jensen, A. A., Lefebvre, S. N., Corringer, P. J., Neyton, J., Chipot, C., Dehez, F., Schoehn, G., & Nury, H. (2018). Conformational transitions of the serotonin 5-HT3receptor. *Nature*, *563*(7730), 275–279. https://doi.org/10.1038/s41586-018-0672-3

Reed, A. E., Curtiss, L. A., & Weinhold, F. (1988). Intermolecular interactions from a natural bond orbital, donor-acceptor viewpoint. *Chemical Reviews*, *88*(6), 899–926. https://doi.org/10.1021/cr00088a005

Reed, A. E., Weinstock, R. B., & Weinhold, F. (1985). Natural population analysis. *Journal of Chemical Physics*, *83*(2), 735–746. https://doi.org/10.1063/1.449486

Reshmy, R., Sajan, D., Kurien Thomas, K., Sulekha, A., Rajasekharan, K. N., Selvanayagam, S., & Alver, Ö. (2012). Synthesis, growth and vibrational spectroscopic study of a novel coumarinoylthiazole. *Spectrochimica Acta. Part A, Molecular and Biomolecular Spectroscopy*, *97*, 1125–1132. https://doi.org/10.1016/j.saa.2012.07.123

Ristimaki, A., Honkanen, N., Jankala, H., Sipponen, P., & Harkonen, M. (1997). Expression of cyclooxygenase-2 in human gastric carcinoma. *Cancer Research*, *57*, 1276–1280.

Rowlinson, S. W., Kiefer, J. R., Prusakiewicz, J. J., Pawlitz, J. L., Kozak, K. R., Kalgutkar, A. S., Stallings, W. C., Kurumbail, R. G., & Marnett, L. J. (2003). A novel mechanism of cyclooxygenase-2 ınhibition ınvolving ınteractions with Ser-530 and Tyr-385. *The Journal of Biological Chemistry*, *278*(46), 45763–45769. https://doi.org/10.1074/jbc.M305481200

Rozas, I., Alkorta, I., & Elguero, J. (2000). Behavior of ylides containing N, O, and C atoms as hydrogen bond acceptors. *Journal of the American Chemical Society*, *122*(45), 11154–11161. https://doi.org/10.1021/ja0017864

Sakurai, K., Urade, M., Noguchi, K., Kishimoto, H., Ishibashi, M., Yasoshima, H., Yamamoto, T., & Kubota, A. (2001). Increased expression of cyclooxygenase-2 in human salivary gland tumors. *Pathology İnternational*, *51*(10), 762–769. https://doi.org/10.1046/j.1440-1827.2001.01280.x

Seibert, K., Zhang, Y., Leahy, K., Hauser, S., Masferrer, J., Perkins, W., Lee, L., & Isakson, P. (1994). Pharmacological and biochemical demonstration of the role of cyclooxygenase 2 in inflammation and pain. *Proceedings of the National Academy of Sciences of the United States of America*, *91*(25), 12013–12017. https://doi.org/10.1073/pnas.91.25.12013

Shirahama, T., & Sakakura, C. (2001). Overexpression of cyclooxygenase-2 in squamous cell carcinoma of the urinary bladder. *Clinical Cancer Research*, *7*, 558–561.

Simon, L. S. (1999). Role and regulation of cyclooxygenase-2 during inflammation, review. *The American Journal of Medicine*, *106*(5B), 37S–42S. https://doi.org/10.1016/s0002-9343(99)00115-1

Simon, S., Duran, M., & Dannenberg, J. (1996). How does basis set superposition error change the potential surfaces for hydrogen-bonded dimers? *Journal of Chemical Physics*, *105*(24), 11024–11031. https://doi.org/10.1063/1.472902

Ślifirski, G., Król, M., & Turło, J. (2021). 5-HT receptors and the development of new antidepressants. *International Journal of Molecular Sciences*, *22*(16), 9015. https://doi.org/10.3390/ijms22169015

Smith, W. L., Garavito, R. M., & De Witt, D. L. (1996). Prostaglandin endoperoxide H synthases (cyclooxygenases)-1 and -2. *The Journal of Biological Chemistry*, *271*(52), 33157–33160. https://doi.org/10.1074/jbc.271.52.33157

Stierand, K., Maass, P. C., & Rarey, M. (2006). Molecular complexes at a glance: Automated generation of two-dimensional complex diagrams. *Bioinformatics (Oxford, England)*, *22*(14), 1710–1716. https://doi.org/10.1093/bioinformatics/btl150

Sylaja, B., Gunasekaran, S., & Srinivasan, S. (2018). Vibrational, NLO, NBO, NMR, frontier molecular orbital and molecular docking studies of diazepam. *Materials Research Innovations*, *22*(6), 361–373.

Tomasi, J., Mennucci, B., & Cammi, R. (2005). Quantum mechanical continuum solvation models. *Chemical Reviews*, *105*(8), 2999–3093. https://doi.org/10.1021/cr9904009

Tucker, O. N., Dannenberg, A. J., Yang, E. K., Zhang, F., Teng, L., Daly, J. M., Soslow, R. A., Masferrer, J. L., Woerner, B. M., Koki, A. T., & Fahey, T. J. 3rd (1999). Cyclooxygenase-2 expression is up-regulated in human pancreatic cancer. *Cancer Research*, *59*(5), 987–990.

van der Bijl, P., & van der Bijl, P. Jr. (2003). Efficacy, safety and potential clinical roles of the COX-2-specific inhibitors. *International Journal of Immunopathology and Pharmacology*. *16*, 17–22.

Veber, D. F., Johnson, S. R., Cheng, H. Y., Smith, B. R., Ward, K. W., & Kopple, K. D. (2002). Molecular properties that influence the oral bioavailability of drug candidates. *Journal of Medicinal Chemistry*, *45*(12), 2615–2623. https://doi.org/10.1021/jm020017n

Wallace, A. C., Laskowski, R. A., & Thornton, J. M. (1995). LIGPLOT: A program to generate schematic diagrams of protein-ligand interactions. *Protein Engineering*, *8*(2), 127–134. https://doi.org/10.1093/protein/8.2.127

Weber, S., Volynets, V., Kanuri, G., Bergheim, I., & Bischoff, S. C. (2009). Treatment with the 5-HT3 antagonist tropisetron modulates glucose-induced obesity in mice. *International Journal of Obesity (2005)*, *33*(12), 1339–1347. https://doi.org/10.1038/ijo.2009.191

Yoosefian, M., Sabaei, S., & Etminan, N. (2019). Encapsulation efficiency of single-walled carbon nanotube for Ifosfamide anti-cancer drug. *Computers in Biology and Medicine*, *114*, 103433. https://doi.org/10.1016/j.compbiomed.2019.103433

Yoshimura, R., Sano, H., Masuda, C., Kawamura, M., Tsubouchi, Y., Chargui, J., Yoshimura, N., Hla, T., & Wada, S. (2000). Expression of cyclooxygenase-2 in prostate carcinoma. *Cancer*, *89*(3), 589–596. https://doi.org/10.1002/1097-0142(20000801)89:3<589::AID-CNCR14>3.0.CO;2-C

Zimmermann, K. C., Sarbia, M., Weber, A. A., Borchard, F., Gabbert, H. E., & Schror, K. (1999). Cyclooxygenase-2 expression in human esophageal carcinoma. *Cancer Research*, *59*, 198–204.